ACS APPLIED MATERIALS & INTERFACES

Research Article

www.acsami.org

Reactive Depth and Performance of an Electrochemical Carbon Nanotube Network as a Function of Mass Transport

Guandao Gao[†,‡] and Chad D. Vecitis*[,†]

[†]School of Engineering and Applied Sciences, Harvard University, Cambridge, Massachusetts 02138, United States

[‡]Key Laboratory of Pollution Processes and Environmental Criteria (Ministry of Education), College of Environmental Science and Engineering, Nankai University, Tianjin 300071, China

Supporting Information

ABSTRACT: Three-dimensional porous electrodes often suffer from diffusional mass-transfer limitations that may be overcome by having the target solution flow through the electrode. Here, we examine the reactive depth and performance of an electrochemical carbon nanotube (CNT) network toward phenol removal and oxidation in the batch and flow configurations where mass transport into the CNT network is predominantly via diffusion and convection, respectively. Scanning electron microscopy depth profile imaging of phenol electropolymerization is used as a direct probe of the reactive depth. In the batch case, electropolymerization is observed to be greatest at the network surface nearest the cathode and decreases linearly to near zero at a depth of 25 μm. In stark contrast, electropolymerization is observed to be independent of the depth in the flow configuration. In agreement with the depth profile results, phenol removal is increased up to 10-fold, the current efficiency is increased by at least 2-fold, and susceptibility toward passivation is reduced in the flow versus batch configuration. Thus, the enhanced electrochemical performance in the flow configuration is partially due to the convective "activation" of the internal CNT network electron-transfer sites that are diffusion-inaccessible.

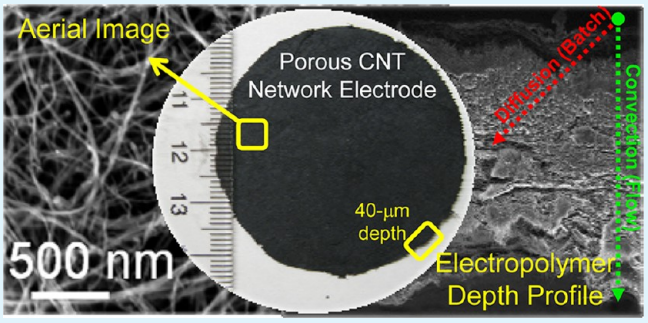

KEYWORDS: *electrochemical filtration, carbon nanotubes, water, phenol, reactive depth*

INTRODUCTION

Carbon nanotubes (CNTs)[1] have a unique set of composite properties including mechanical strength,[2] one-dimensional conductivity,[3] high specific surface area and aspect ratio,[4] and chemical stability.[5] In turn, free-standing CNT networks, which can be simply formed by vacuum filtration,[6] have a similar set of properties. Thus, three-dimensional porous CNT networks make excellent substrates for electrochemical processes[7] and have been investigated for use in batteries,[8] fuel cells,[9] solar energy conversion,[10] sensors,[11] and water treatment.[12] Electrochemical CNT networks are also reported to be advantageous[13,14] compared to conventional carbon-based supports such as activated carbon cloths and felts because of their high porosity (>85%), increased fraction of easily accessible surface sites (>95% vs ~30%),[15] increased conductivity,[3] near-ideal electron-transfer kinetics,[16,17] and corrosion resistance.[5] However, diffusion limitations may reduce the reactive depth of a porous three-dimensional CNT network electrode even for micrometer-scale depths. For example, a recent study observed diffusion limitations for a three-dimensional electrode of 1.7-μm thickness.[18]

One strategy to overcome the diffusion limitations of a conventional bipolar electrode configuration (batch) is to flow the electrolyte solution either by, tangential to, or through, perpendicular to (flow), the porous three-dimensional electrode (Figure 1). For example, previous studies of flow-through metal[19] and carbon[20,21] felts, foams, and cloth electrodes for metal recycling and contaminant oxidation reported linear increases in the current and mass-transfer coefficients with increasing fluid velocity. The slope of the linear increase of the mass-transfer coefficient with fluid velocity is a function of both the pore diameter (diffusion length) and porous electrode depth (plug-flow reactor length). However, these porous electrodes are quite thick (>1 mm), have large pores (>10 μm), require special reactors, and thus tend to perform better in the flow-by configuration because of the ohmic drop across the porous electrode thickness.[22] More recent investigations have suggested the same flow enhancements may be active for porous CNT-based electrodes. A granular CNT seepage electrode for dye wastewater oxidation displayed a 1.6-fold improvement in mass transfer and a 3-fold improvement in the current efficiency when operated in the flow configuration compared to the batch configuration.[12] Similarly, an electrochemical CNT network of only 40-μm thickness produced from well-dispersed CNTs displayed a 6-fold increase in the

Received: August 20, 2012
Accepted: October 29, 2012
Published: October 29, 2012

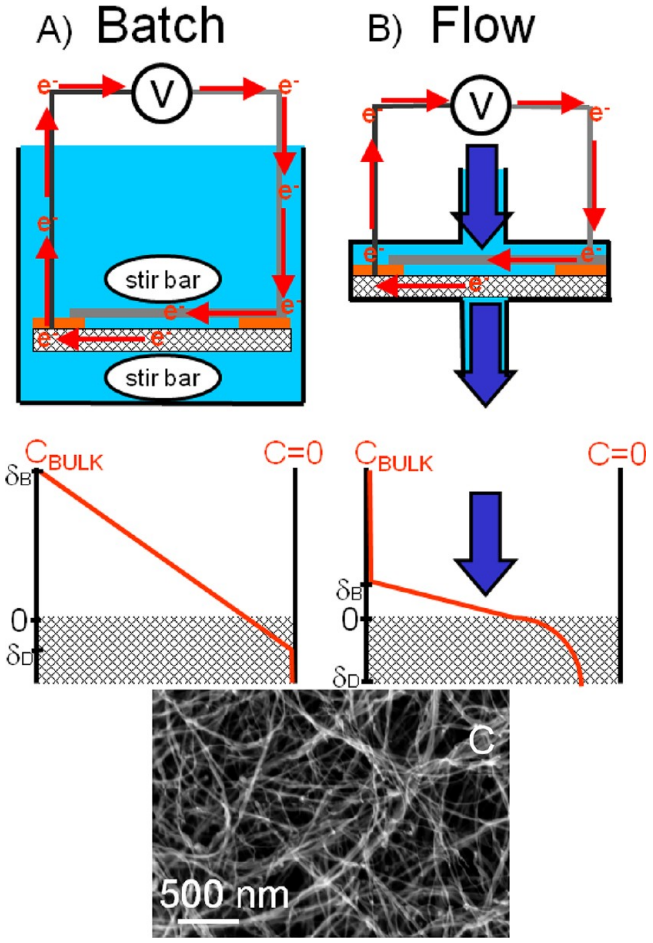

Figure 1. Diagrams and images of the electrochemical CNT network and configurations. Electrochemical (A) batch and (B) flow cell configurations and corresponding hypothetical near and internal CNT network phenol concentration gradients during steady-state electrolysis. (C) Aerial SEM image of a CNT network.

current and aqueous dye oxidation when operated in the flow configuration compared to the batch configuration.[23]

The enhanced flow-through electrochemistry can be attributed to two possible mechanisms: see the concentration gradients in Figure 1. The first mechanism is the increase in mass transfer to the porous electrode surface by convective reduction of the diffusion boundary layer (δ_B). In the batch system, the boundary layer will steadily grow after onset of electrochemistry to some steady-state length of up to around 1 mm, δ_B(batch) ~ 1 mm, as estimated by the equation derived by Levich for the average diffusion boundary layer thickness of a flat plate electrode due to natural convection.[24,25] In the flow system, this boundary layer will be reduced with increasing flow rate, i.e., steady-state balance between forward convection and back diffusion, and eventually converge to the electrode pore radius, $r_{pore} \leq \delta_B(\text{flow}) \leq \delta_B(\text{batch})$. The second mechanism is the convective "activation" of the internal electron-transfer sites, i.e., increase in the reactive depth (δ_D). In the batch system, only a fraction of the depth and thus electron-transfer sites will be accessible by diffusion. In the flow system, convection through the electrode should in theory activate all of the electron-transfer sites if the current can be effectively transported throughout the porous electrode.

Here, we report on the experimental investigation into the latter flow-through enhancement mechanism for an electrochemical CNT network (r_{pore} ~ 50 nm; d ~ 40 μm) using phenol removal and oxidation as both a direct and indirect probe. Phenol was selected as a target molecule for oxidation because it is an industrial chemical produced at 10^7 tons year^{-1} [26] and a common environmental contaminant found at >400 U.S. EPA Superfund sites,[27] can act as a sacrificial-electron donor for electrochemical H_2 production,[28] and significantly electropolymerizes onto CNTs at anode potentials <1.85 V vs Ag/AgCl.[29] The last characteristic is crucial because it will be used here as a direct analytical tool of the electrochemically reactive CNT network depth. Electrochemical experiments are completed in both batch and flow configurations for comparison, and conditions are designed such that the electrolysis time, electrolyzed volume, and electrode properties are identical in both configurations. The extent of electrochemical phenol polymerization onto the CNTs as measured by scanning electron microscopy (SEM) is used as a direct probe of the reactive depth. The extents of electrochemical phenol removal and current measurements are used for an indirect performance comparison. Electrochemical impedance spectroscopy (EIS) of the CNT networks is used to support previous flow enhancement observations and evaluate the polymer and precipitant passivation mechanisms.

MATERIALS AND METHODS

Chemicals. All chemicals, phenol (PhOH; C_6H_6O), sodium sulfate (Na_2SO_4), and hydrochloric acid (concentrated HCl), were reagent grade except dimethyl sulfoxide (DMSO), which was spectrophotometric grade, and were purchased from Sigma-Aldrich (St. Louis, MO).

CNT Selection, Purification, and Network Preparation. The electrochemical CNT network and method used in this study have been previously described in detail.[30,31] Briefly, the CNTs used in this study were purchased from NanoTechLabs (Yadkinville, NC) and selected because of their low cost of \$10 g^{-1} (<\$1 g^{-1} if purchased at ton scale), resulting in a cost of 15¢ per network used in this study. The CNT cost is 10 times less than that of the porous poly(tetrafluoroethylene) (PTFE) membrane used to support the CNT network at \$1.5 per film. The CNTs were multiwalled CNTs of 5−7 walls on average, 15−20 nm in diameter, and 100 μm in length.[32] The CNTs were first purified by calcination at 400 °C for 1 h in a tube furnace (Thermolyne, 21100) to remove any amorphous and non-CNT carbon impurities. Calcination was followed by a subsequent acid treatment by stirring in concentrated HCl at 70 °C for >12 h to remove residual metal oxide catalyst for optimal CNT surface chemistry with minimal CNT oxidation.[33] After heating, the sample was cooled to room temperature and vacuum-filtered through a 5-μm PTFE membrane (JMWP, Omnipore, Millipore) to collect the CNTs. The CNTs were then washed with Milli-Q deionized (DI) water until the filter effluent pH was neutral. The sample was then oven-dried at 100 °C before further use. The CNTs were then dispersed at 0.5 mg mL^{-1} in DMSO by probe ultrasound (Branson) at 400 W L^{-1} for 15 min, and then 30 mL of the DMSO CNT was immediately vacuum-filtered onto a 5-μm-pore-size PTFE membrane (JMWP, Omnipore, Millipore) and sequentially washed with 100 mL of EtOH, 100 mL of 1:1 DI water/EtOH, and 250 mL of DI water to remove any residual DMSO. The CNT network of 40 μm depth was then placed in a modified polycarbonate filter casing (Whatman) with a titanium anodic connector ring and a perforated stainless steel cathode separated by a silicon rubber ring (Figures 1 and S1 in the Supporting Information).

Electrochemical Batch and Flow Experiments. Schematic depictions and images of the batch and flow configurations can be found in Figures 1 and S1 in the Supporting Information. The batch cell had the top and bottom of the polycarbonate flow cell removed such that stirbars could be operated on both sides for maximum convection tangential to the CNT electrodes. The batch system had a

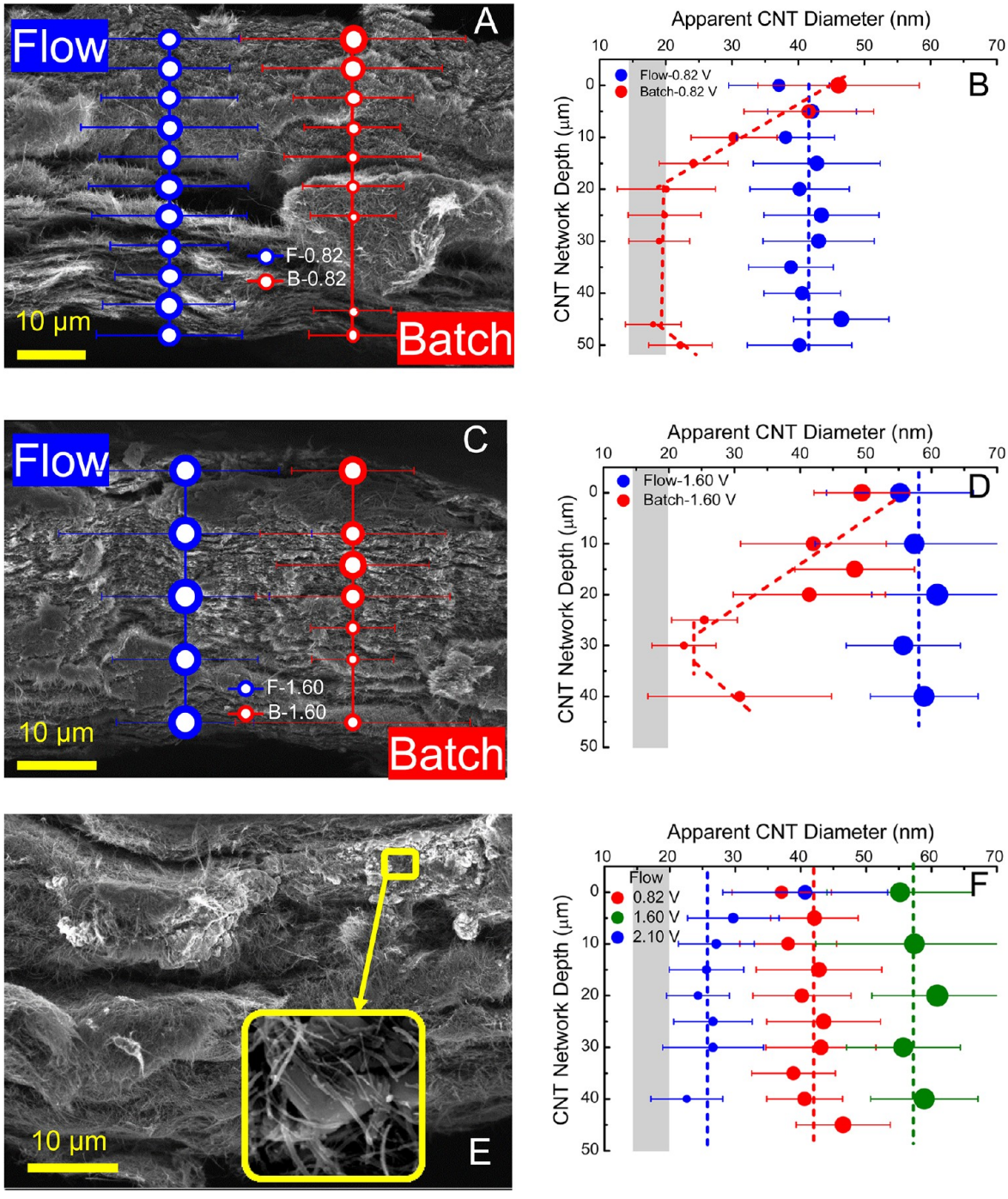

Figure 2. Phenol polymerization as a function of the electrochemical CNT network depth in the batch and flow configurations. Electrochemical conditions are the same as those in Figure 1. SEM cross-sectional images of an electrolyzed CNT network at (A) 0.82 V and (C) 1.6 V anode potentials with bubble plots of the CNT diameter in the flow (blue) and batch (red) configurations. Apparent CNT diameter as a function of the network depth for phenol electrolysis at (B) 0.82 V and (D) 1.6 V anode potentials in the flow (blue) and batch (red) configurations. The gray bars represent the range of fresh CNT diameters. (E) SEM image of a CNT network electrolyzed at 2.1 V in the flow configurations to exemplify salt formation, and the inset is a magnification of the dense salt particles in the top layer of the CNT network. (F) Apparent CNT diameter as a function of the network depth for phenol electrolysis at 0.82 V (red), 1.60 V (green), and 2.10 V (blue) in the flow configuration. Note that the circle diameter is scaled according to the relative apparent CNT diameter.

total volume of 170 mL and was electrolyzed for 106 min. The flow configuration was operated at a flow rate of 1.6 mL min^{-1} through the CNT network for 106 min to electrolyze a total volume of 170 mL. Thus, the electrolysis time (106 min) and volume (170 mL) were equivalent for the two systems. The solution to be treated consisted of 1 mM phenol in a 100 mM sodium sulfate electrolyte with an initial pH of around 6. Experiments were completed in both systems at anode potentials of 0.82, 1.6, and 2.1 V vs Ag/AgCl. The influent and effluent phenol concentrations were measured at various time points during electrolysis by a total organic carbon (TOC) analyzer (Shimadzu) and by a UV−visible spectrophotometer (Agilent) at 254 nm. The steady-state current and anode potential were constantly measured during electrolysis with a potentiostat (CHI 604D). The reported values are averages of at least two experiments. Electro-

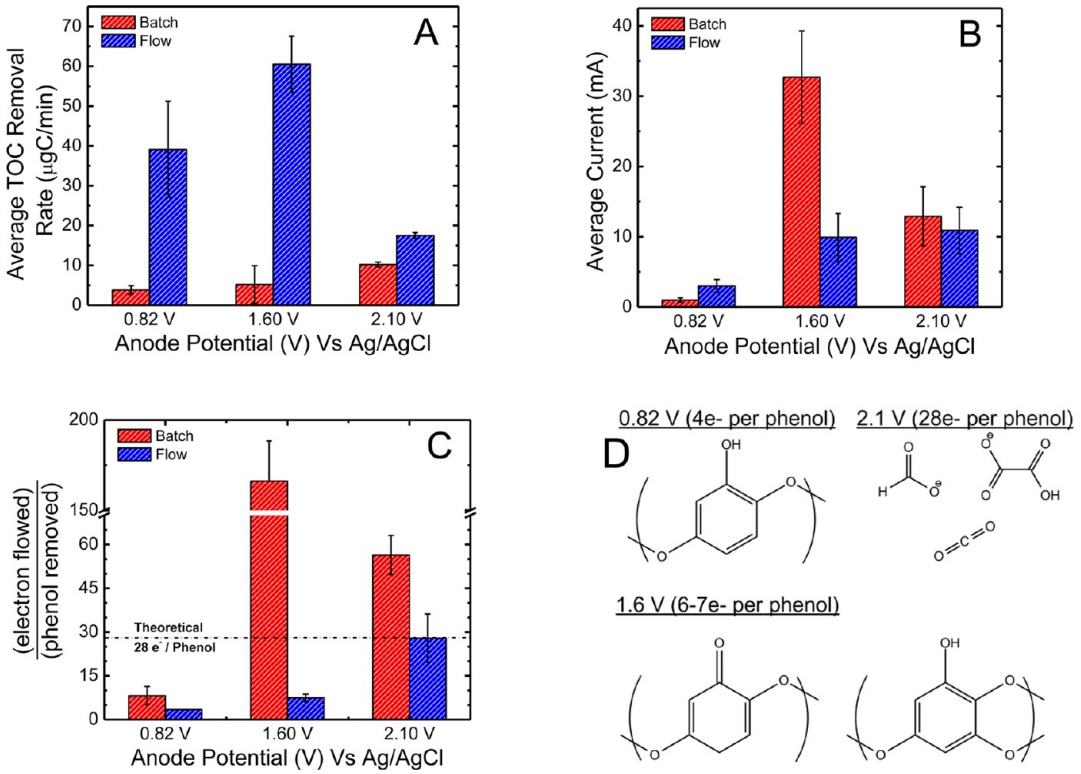

Figure 3. Comparison of the electrochemical batch and flow cell configurations for phenol removal, oxidation kinetics, and current efficiency: (A) average TOC removal rate in μgC min^{-1}, (B) average current in mA, (C) average phenol oxidation current efficiency in electrons per phenol, and (D) plausible reaction products as a function of anode potential. Electrochemical conditions (blue bars) were t = 106 min, $[PhOH]_{in}$ = 1.0 mM, and $[Na_2SO_4]$ = 100 mM at anode potentials of 0.82, 1.60, and 2.10 V. The batch reactor was of 170-mL volume, and the flow system had J = 1.6 mL min^{-1}. Note that the electrolysis time and volume treated are the same for the batch and flow configurations.

chemical characterization and SEM depth profiles of the CNT networks were completed both pre- and postelectrolysis as described in detail below.

Electrochemical Characterization. The CNT networks pre- and postelectrolysis were electrochemically characterized with a CHI 604D electrochemical workstation (CHI, USA). The CNT network was employed as the working electrode, a stainless steel cathode was used as the counter electrode, and a 1 M Ag/AgCl solution was used as the reference electrode. Thus, all anode potentials listed in the text and figures are with respect to Ag/AgCl. Batch/flow and solution (1 mM PhOH and 100 mM Na_2SO_4) conditions similar to those of the electrolysis experiments were used for the electrochemical characterization. The used (electrolyzed) solutions were replaced with fresh (nonelectrolyzed) solutions prior to characterization. EIS was completed at a potential amplitude of 5 mV scanned over a frequency range of 0.1−10^6 Hz. The resultant data were simulated with Nyquist and/or Bode plots. The *Zview* software (Scribner, Southern Pines, NC) was used for quantitative analysis of the EIS data to determine individual capacitor and resistor values.

SEM Analysis. The apparent CNT diameters were measured by SEM (Zeiss Supra field-emission scanning electron microscopy, Harvard Center for Nanoscale Systems). The CNT networks were prepared for SEM by cutting a 0.5 × 0.5 cm^2 sample from the center of the network and then using a precision knife to cut the sample in two. Cross-sectional depth profile images of the CNT network were completed by starting with an initial image at the top of the CNT network and then shifting the position of the SEM sample stage by 5-to-10-μm increments to take the subsequent image until the bottom of the sample was observed. Micrographs were analyzed with *ImageJ* software to determine the apparent CNT diameter. Measurements were the average of at least 100 measurements from at least two network images. Diameter measurements were made manually and then tabulated and analyzed automatically by the *ImageJ* software.

RESULTS AND DISCUSSION

Flow-Enhanced Anodic CNT Network Reactive Depth.

To examine the electrochemically active depth of the anodic CNT network in the flow and batch configurations, the extent of phenol polymerization, which has been previously reported to result in growth of the apparent CNT diameter by as much as 30 nm,[29] was used as an analytical probe. SEM images of the flow (blue circles) and batch (red circles) anodic CNT network cross sections at 0.82, 1.6, and 2.1 V along with the apparent CNT diameter depth profiles (images every 5−10 μm) are presented in Figures 2 and S2 in the Supporting Information. The gray bar represents the range of fresh (preelectrolysis) CNT diameters, and thus any diameter greater than the gray bar is representative of polymer formation,[29] and the dashed lines are eye guides. It is quite obvious in parts B (0.82 V) and D (1.6 V) of Figure 2 that the apparent CNT diameter and thus extent of polymerization are similar through the whole depth of the CNT network electrolyzed in the flow configuration. In stark contrast, the extent of polymerization in the batch configuration is only similar to the flow at the surface nearest the cathode and then decreases linearly with a network depth for 20−25 μm where there is minimal polymerization. A slight increase in polymerization is observed at the CNT network surface furthest from the cathode as well. The linear decrease in polymerization with the network depth is indicative of a linear decrease in the phenol concentration with depth and representative of a diffusion-controlled concentration gradient. Thus, in the flow configuration, the convection through the CNT network acts to constantly replenish fresh phenol to "all" of the electrode surface areas and effectively "activate" the

diffusion-inaccessible internal electron-transfer sites toward phenol oxidation.

A quantitative comparison of the extent of polymer growth in the flow versus batch systems may give insight into the importance of the internal electron-site activation mechanism. The polymer volume can be estimated by $\pi(r_{app}^2 - r_{cnt}^2)l$, where r_{app} is the CNT diameter postpolymerization, r_{cnt} is the average fresh CNT diameter, and l is the CNT length. Assuming l is constant, the ratio of the flow-to-batch polymer volumes can be calculated by $(r_{app,f}^2 - r_{cnt}^2)/(r_{app,b}^2 - r_{cnt}^2)$. The average flow-to-batch polymer volume ratios over the whole network depth are 2.7 (0.82 V) and 2.9 (1.6 V). For comparison, at 0.82 and 1.6 V and 30-μm depth where the flow and batch diameters have the greatest disparity, the flow-to-batch polymer volume ratios are 13.2 and 14.6, respectively. Indicating quantitatively that the flow-through electrochemistry enhancement could be significantly (>4-fold) increased by simply increasing the CNT network electrode depth to greater than the 40-μm depth used in this study.

An SEM image of the anodic CNT network electrolyzed at a potential of 2.1 V is presented in Figure 2E, and its apparent CNT diameter depth profile is compared to those electrolyzed at 0.82 and 1.6 V in Figure 2F. It is of note that the 2.1 V CNT diameter is similar to the 1.6 V CNT diameter at the network surface near the cathode but decreases rapidly to ~25 nm for most of the depth, 10−40 μm. The lower extent of CNT diameter growth at 2.1 V is due to the ability of this potential to crack the aromatic ring and thus destroy any polymerizing phenoxide radicals,[34,35] as will be discussed later. The larger-diameter CNTs on the surface nearest the cathode are more likely due to salt precipitation, e.g., sulfate oxidation to persulfate,[28] which has a significantly lower water solubility of 1 mM.[29] Carbonate oxidation to peroxydicarbonate ($C_2O_6^{2-}$) or peroxocarbonate (CO_4^{2-}) may also be responsible for the precipitate formation and would explain the unknown carbon-containing precipitates observed in a previous work.[29] Large and numerous near-surface salt crystals are observed in the SEM of the 2.1 V CNT network (Figure 2E and inset). The CNT diameter of the 1.6 V sample is greater than the 0.82 V sample because 1.6 V is still too low to break the aromatic ring, so polymerizing phenolic radicals will still be the dominant electrooxidation product and the phenol oxidation kinetics will be increased at the higher potential, i.e., $k = i/n \sim E_{app} - E^0$.[25]

Flow-Enhanced Anodic CNT Network Efficacy and Efficiency. To support the depth profile results, the average TOC, average current, electrons flowed per phenol removed, and representative electrooxidation products are presented in Figure 3 for CNT network anode potentials of 0.82, 1.6, and 2.1 V for the batch (red) and flow (blue) configurations. At all potentials, the phenol TOC removal rate in the flow configuration is greater than that in the batch configuration (Figure 3A), in agreement with the results in Figure 2. The 0.82 and 1.6 V data show a nearly 10-fold increase of phenol removal in the flow configuration compared to the batch configuration, which is greater than the 6-fold flow enhancement observed for methyl orange decolorization under similar conditions.[23] At 2.1 V, the enhancement is only 1.7-fold, suggesting a change in the phenol electrooxidation mechanism from polymerization to mineralization, as will be discussed later, and again in agreement with the depth profile results that indicated minimal polymerization at 2.1 V.

In contrast to the TOC removal rate, at 1.6 and 2.1 V, the average current is greater in the batch configuration compared to the flow configuration (Figure 3B). Because the reactor configuration would have a minimal effect on the phenol electrooxidation mechanism, the increased current in the batch system suggests that alternative (nonphenol) electrochemistry is occurring at the internal anodic CNT network surface area inaccessible to phenol diffusion. For example, a previous study reported the CNT electrooxidation of water to oxygen ($2H_2O + 4h^+ \rightarrow O_2 + 4H^+$, $E^0_{Ag/AgCl}$ = 1.03 V)[36] at 1.1 V anode potential.[23] Thus, the increased current and decreased phenol removal at 1.6 V in the batch configuration is likely due to water oxidation in regions of the CNT network inaccessible to phenol diffusion. Similarly at 2.1 V, the two-electron oxidation of the sulfate electrolyte to persulfate ($2SO_4^{2-} + 2h^+ \rightarrow S_2O_8^{2-}$, $E^0_{Ag/AgCl}$ = 1.83 V) or produced carbonate to peroxodicarbonate, in agreement with observed salt precipitation in Figure 2E, and the one-electron oxidation of water to the hydroxyl radical ($H_2O/HO^- + h^+ \rightarrow {}^{\bullet}OH + H^+$, $E^0_{Ag/AgCl}$ = 2.5/1.8 V) become thermodynamically viable. The lower average current at 2.1 versus 1.6 V may be due to a lesser number of electrons transferred per reaction, but is more likely due to the increased charge-transfer resistance from precipitate formation, as will be discussed in the following section.

The electrons flowed per phenol removed is presented in Figure 3C. The dashed horizontal line represents the max electrons (28) that can be removed per phenol during mineralization, i.e., complete oxidation to CO_2 ($C_6H_6O + 7O_2 + 28h^+ \rightarrow 6CO_2 + 3H_2O$). It is of note that, for all potentials in the flow configuration, the average electrons flowed per phenol is at least half that of the batch configuration and at or below the theoretical value for complete oxidation. This result indicates that the flow configuration has a greater current efficiency than the batch configuration. This is likely due to the constant convective replenishment of phenol at the CNT surface for direct oxidation, the most efficient electro-oxidation mechanism. The lower electrons flowed per phenol but greater removal at 0.82 and 1.6 V compared to 2.1 V is a result of oxidative phenol polymerization to polyphenoxide, which coats the CNTs (Figure 2).[29] In agreement with previous phenol electrooxidation studies that observed anode potentials ≥1.85 V were necessary for phenol aromatic ring opening, yielding small organic acids.[34]

The electrons flowed per phenol and electropolymerization observed at 0.82 and 1.6 V result in a significant reduction in the number of possible phenol electrooxidation products. For example, at 0.82 V, four electrons flowed per phenol could only result from either oxidation of two C−H bonds to two C−O bonds or one C−H to one C−O and C−OH to C═O. Also, if polymerization is active, then only the former mechanism is possible because every phenolic monomer needs to be bonded to two other phenolic monomers (Figure 3D). A similar argument can be made for the suggested electrooxidation products at 1.6 V, where the only possible variations in both cases may be in the positions of the C−H to C−O bond oxidations. The electrooxidation mechanism at 2.1 V is quite different because this potential is sufficient enough to open the aromatic ring, thus eliminating any polymerizing phenoxide radicals, generate strong one-electron oxidants such as the hydroxyl and sulfate radicals,[37] and directly oxidize recalcitrant organic acids such as oxalate to CO_2.[38] The near-complete mineralization of phenol at 2.1 V and predominant production of small organic acids and carbon dioxide are supported by the electrons flowed per phenol in the flow system at 28 ± 8 e^- per phenol that falls on the theoretical maximun for complete

oxidation. The greater number of electrons removed per phenol at 2.1 V is likely responsible for the reduction in the phenol removal rate because electron transfer becomes more important than mass transfer.

The results presented in Figure 3 support the conclusion that the flow configuration is superior to the batch configuration for anodic CNT networks with regards to both electrooxidative phenol removal and current efficiency. The greater efficacy of the flow configuration is a result of the increased phenol mass transfer to the internal electrode surface area in the flow (convective) configuration compared to the batch (diffusive) configuration.

Flow-Enhanced Anodic CNT Network Passivation Reduction. Experimental EIS was completed in the presence of the target solution for a fresh CNT network, the 0.82 V network postelectrolysis, and the 2.1 V network postelectrolysis and is displayed as points in Figure 4. The EIS data were modeled using the *Zview* software and presented as dashed lines in Figure 4 with the corresponding fitted parameters in Table 1. Three different model circuits were used to fit the data for (1) all batch, (2) fresh and 0.82 V in flow, and (3) 2.1 V in flow. In these model circuits, R_s is the solution resistance in

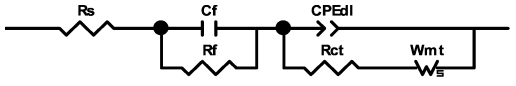

(1)

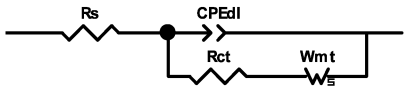

(2)

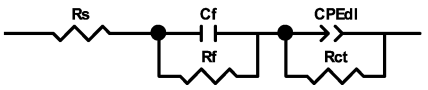

(3)

ohms, R_f the film resistance in ohms, R_{ct} the charge-transfer resistance in ohms, W_{mt} the mass-transfer resistance in ohms, C_f the film capacitance in microfarads, and CPE_{dl} the double-layer capacitance in microfarads. In all cases, the double-layer capacitance is the dominant capacitor. The double-layer capacitance decreases in the batch system from the fresh (141 μF) to 0.82 V (98 μF) to 2.1 V (65 μF), indicating a loss of capacitive surface area, i.e., burial of the electroactive sites by the polymer or precipitant. In contrast, the double-layer capacitance for the three flow networks is similar at 44 μF and lesser than all of the batch samples, suggesting that the convective flow through the network may cause near-surface turbulence that reduces the double-layer Debye length.

The anodic CNT network resistance is dominated by the mass-transfer and electron-transfer resistances, as expected. The dominant resistor at 0.82 and 2.1 V electrolyzed networks gives insight into the different passivation mechanisms for the polymer and precipitate (Figure 4D). The total 0.82 V network resistance is dominated by increases in the mass-transfer resistance, 10-fold in flow and 8-fold in batch, compared to fractional increases in the charge-transfer resistance. This indicates that, although the polymer coats the CNTs, the electron-transfer sites are still active and that the primary mode of polymer passivation is to add a diffusional resistance; i.e., diffusion through the polymer to the electrochemically active surface sites is much slower than diffusion through a free

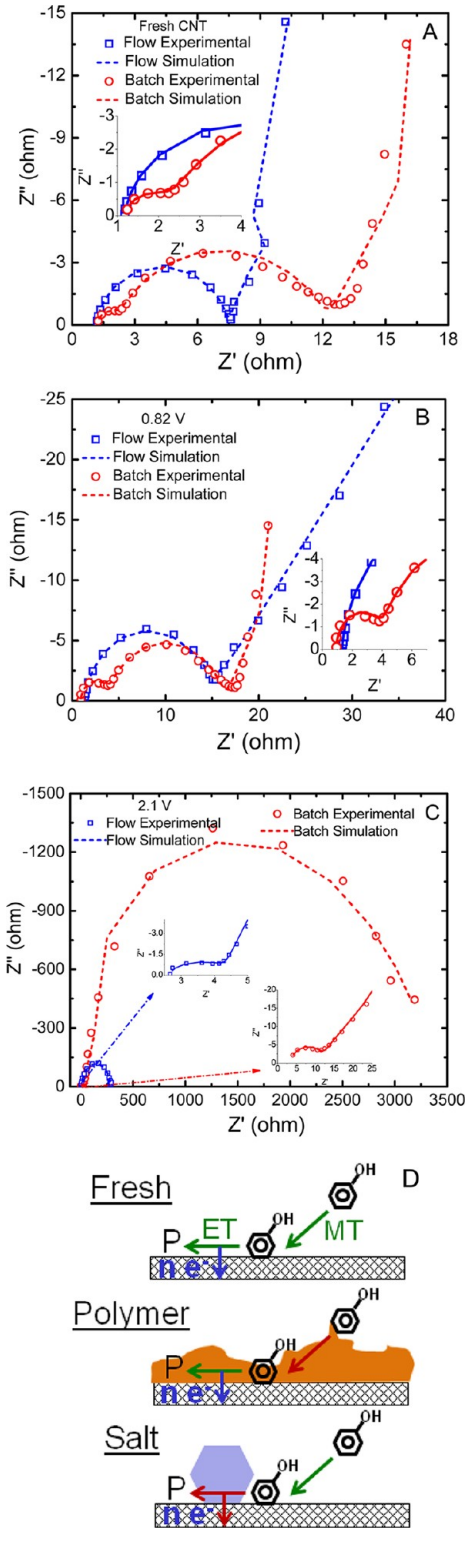

Figure 4. Experimental and simulated EIS for the flow and batch configurations: (A) EIS of fresh CNT; (B) EIS of the CNT network electrolyzed at an anode potential of 0.82 V; (C) EIS of the CNT network electrolyzed at an anode potential of 2.1 V. The EIS spectra were completed using a potential amplitude of 5 mV over a frequency range of 0.1−10^6 Hz and were simulated using the *Zview* software. In all figures, the experimental and simulated EIS data for the flow configuration are plotted with blue squares and blue dashed lines, respectively, and those for the batch configuration with red circles and red dashed lines, respectively. The insets are magnifications of the initial part of the spectra.

dx.doi.org/10.1021/am301724n | *ACS Appl. Mater. Interfaces* 2012, 4, 6096−6103

Table 1. Simulated EIS Resistance and Capacitance Values[a]

electrolysis conditions		R_s (Ω)	C_f (μF)	R_f (Ω)	CPE_{dl} (μF)	R_{ct} (Ω)	W_{mt} (Ω)
fresh CNT network	flow	1.2	n/a	n/a	44.1	6.2	18.5
	batch	1.2	1.9	0.9	141.0	10.0	28.8
0.82 V postelectrolysis	flow	1.3	n/a	n/a	43.6	10.2	**187.8**
	batch	0.9	0.9	2.8	97.9	13.6	**233.7**
2.10 V postelectrolysis	flow	2.7	1.0	1.6	44.6	**285.3**	n/a
	batch	3.5	0.1	7.8	65.3	**2992**	431.3

[a] R_s is the solution resistance, C_f is the film capacitance, R_f is the film resistance, CPE_{dl} is the double-layer capacitance, R_{ct} is the charge-transfer resistance, and W_{mt} is the mass transfer resistance.

solution. In contrast, salt precipitation at 2.1 V predominantly results in massive increases in the charge-transfer resistance, 46-fold in flow and 300-fold in batch, with a disappearance of the mass-transfer resistance in the flow and a 15-fold increase in the batch. The precipitate will be much denser ($\rho_{Na_2SO_4}$ = 2.4 g cm^{-3} vs ρ_{poly} = 1.05 g cm^{-3})[36] and significantly more insulating than the polymer coating, resulting in "deactivation" of any precipitate-coated electron-transfer sites. Also, because a greater number of electrons are transferred per phenol at 2.1 V, the electron-transfer step gains greater importance. It is of note that, at both 0.82 and 2.1 V, the flow network underwent a lesser absolute increase in total resistance than the batch, indicating that the flow configuration is less susceptible to passivation. In particular, the convective flow reduced the precipitate charge-transfer resistance by over 1 order of magnitude compared to the batch. This is likely a result of the spreading of the electrochemistry over a greater CNT surface area, in turn lessening the average local accumulation of surface passivants and the convective washing of the CNT network electrode.

CONCLUSION

In summary, we have shown that an electrochemical CNT network operated in the flow configuration is superior to that in a batch configuration with regards to the extent of phenol extraoxidation (up to 10-fold), current efficiency (greater than 2-fold), and susceptibility to passivation. Depth profiles of phenol electropolymerization provide direct evidence that the convective flow "through" the CNT network effectively "activates" the internal electron-transfer sites that were diffusion-inaccessible in the batch system and indicate that one strategy to increase this flow enhancement is to simply increase the depth of the CNT network. The higher current efficiency in the flow configuration is due to the predominance of the inherently more efficient direct (compared to indirect) phenol electrooxidation mechanism. The lower passivation in the flow configuration is likely a result of the convective flow sweeping away the passivating material. These results clearly demonstrate the advantages of using a liquid flow perpendicular to a porous three-dimensional electrode and have strong implications for Faradaic electrochemical processes such as those used in oxidative water treatment.

ASSOCIATED CONTENT

Supporting Information

Images of the electrochemical filtration setup, representative 100× magnification depth profile SEM images, and linear sweep voltammetry. This material is available free of charge via the Internet at http://pubs.acs.org.

AUTHOR INFORMATION

Corresponding Author

*E-mail: vecitis@seas.harvard.edu. Phone: (617) 496-1458.

Notes

The authors declare no competing financial interest.

ACKNOWLEDGMENTS

G.G. is thankful for a Harvard GSAS Visiting Fellow Scholarship and a Chinese Scholarship. We thank Harvard's Center for Nanoscale Systems for SEM. We thank the Korean Institute of Geosciences and Mineral Resources for funding (Grant 214551-01).

REFERENCES

(1) Iijima, S. *Nature* **1991**, *354* (6348), 56−58.
(2) Pantano, A.; Boyce, M. C.; Parks, D. M. *Phys. Rev. Lett.* **2003**, *91* (14), 145504-1−145504-4.
(3) Gooding, J. J.; Wibowo, R.; Liu, J. Q.; Yang, W. R.; Losic, D.; Orbons, S.; Mearns, F. J.; Shapter, J. G.; Hibbert, D. B. *J. Am. Chem. Soc.* **2003**, *125* (30), 9006−9007.
(4) Peigney, A.; Laurent, C.; Flahaut, E.; Bacsa, R. R.; Rousset, A. *Carbon* **2001**, *39* (4), 507−514.
(5) Wang, X.; Li, W. Z.; Chen, Z. W.; Waje, M.; Yan, Y. S. *J. Power Sources* **2006**, *158* (1), 154−159.
(6) Brady-Estevez, A. S.; Kang, S.; Elimelech, M. *Small* **2008**, *4* (4), 481−484.
(7) Li, J.; Cassell, A.; Delzeit, L.; Han, J.; Meyyappan, M. *J. Phys. Chem. B* **2002**, *106* (36), 9299−9305.
(8) Reddy, A. L. M.; Shaijumon, M. M.; Gowda, S. R.; Ajayan, P. M. *Nano Lett.* **2009**, *9* (3), 1002−1006.
(9) Girishkumar, G.; Vinodgopal, K.; Kamat, P. V. *J. Phys. Chem. B* **2004**, *108* (52), 19960−19966.
(10) Kim, Y. K.; Park, H. *Energy Environ. Sci.* **2011**, *4* (3), 685−694.
(11) Li, J.; Ng, H. T.; Cassell, A.; Fan, W.; Chen, H.; Ye, Q.; Koehne, J.; Han, J.; Meyyappan, M. *Nano Lett.* **2003**, *3* (5), 597−602.
(12) Yang, J.; Wang, J.; Jia, J. P. *Environ. Sci. Technol.* **2009**, *43* (10), 3796−3802.
(13) Liu, H. S.; Song, C. J.; Zhang, L.; Zhang, J. J.; Wang, H. J.; Wilkinson, D. P. *J. Power Sources* **2006**, *155* (2), 95−110.
(14) McCreery, R. L. *Chem. Rev.* **2008**, *108* (7), 2646−2687.
(15) Niu, C. M.; Sichel, E. K.; Hoch, R.; Moy, D.; Tennent, H. *Appl. Phys. Lett.* **1997**, *70* (11), 1480−1482.
(16) Nugent, J. M.; Santhanam, K. S. V.; Rubio, A.; Ajayan, P. M. *Nano Lett.* **2001**, *1* (2), 87−91.
(17) Banks, C. E.; Moore, R. R.; Davies, T. J.; Compton, R. G. *Chem. Commun.* **2004**, *16*, 1804−1805.
(18) Milczarek, G.; Inganas, O. *Science* **2012**, *335* (6075), 1468−1471.
(19) Marracino, J. M.; Coeuret, F.; Langlois, S. *Electrochim. Acta* **1987**, *32* (9), 1303−1309.
(20) Coeuret, F.; Vilar, E. O.; Cavalcanti, E. B. *J. Appl. Electrochem.* **2002**, *32* (10), 1175−1182.
(21) Oren, Y.; Soffer, A. *Electrochim. Acta* **1983**, *28* (11), 1649−1654.

(22) Trainham, J. A.; Newman, J. *Electrochim. Acta* **1981**, *26* (4), 455−469.
(23) Liu, H.; Vecitis, C. D. *J. Phys. Chem. C* **2012**, *116* (1), 374−383.
(24) Levich, V. G. *Physicochemical Hydrodynamics*; Prentice-Hall: Englewood Cliffs, NJ, 1962.
(25) Bard, A. J.; Faulkner, L. R. *Electrochemical Methods: Fundamentals and Applications*, 2nd ed.; John Wiley & Sons: New York, 2001; p 833.
(26) Weber, M.; Weber, M. *Phenols*; Springer-Verlag: Berlin, 2010.
(27) http://cumulis.Epa.Gov/supercpad/cursites/srchsites.Cfm.
(28) Park, H.; Vecitis, C. D.; Hoffmann, M. R. *J. Phys. Chem. C* **2009**, *113* (18), 7935−7945.
(29) Gao, G. D.; Vecitis, C. D. *ACS Appl. Mater. Interfaces* **2012**, *4* (3), 1478−1489.
(30) Vecitis, C. D.; Gao, G. D.; Liu, H. *J. Phys. Chem. C* **2011**, *115* (9), 3621−3629.
(31) Vecitis, C. D.; Schnoor, M. H.; Rahaman, M. S.; Schiffman, J. D.; Elimelech, M. *Environ. Sci. Technol.* **2011**, *45* (8), 3672−3679.
(32) Kang, S.; Herzberg, M.; Rodrigues, D. F.; Elimelech, M. *Langmuir* **2008**, *24* (13), 6409−6413.
(33) Gao, G.; Vecitis, C. D. *Environ. Sci. Technol.* **2011**, *45* (22), 9726−9734.
(34) Iniesta, J.; Michaud, P. A.; Panizza, M.; Cerisola, G.; Aldaz, A.; Comninellis, C. *Electrochim. Acta* **2001**, *46* (23), 3573−3578.
(35) Kreh, R. P.; Tadros, M. E.; Hand, H. M.; Cockerham, M. P.; Smith, E. K. *J. Appl. Electrochem.* **1986**, *16* (3), 440−446.
(36) *CRC Handbook of Chemistry and Physics*, 91st ed.; CRC Press: Boca Raton, FL, 2011.
(37) Wardman, P. J. *J. Phys. Chem. Ref. Data* **1989**, *18* (4), 1637−1755.
(38) Vecitis, C. D.; Lesko, T.; Colussi, A. J.; Hoffmann, M. R. *J. Phys. Chem. A* **2010**, *114* (14), 4968−4980.